JCI insight

Minimally invasive method for the point-of-care quantification of lymphatic vessel function

Anna K. Polomska, … , Jean-Christophe Leroux, Michael Detmar

JCI Insight. 2019;4(4):e126515. https://doi.org/10.1172/jci.insight.126515.

Technical Advance | Dermatology | Vascular biology

Graphical abstract

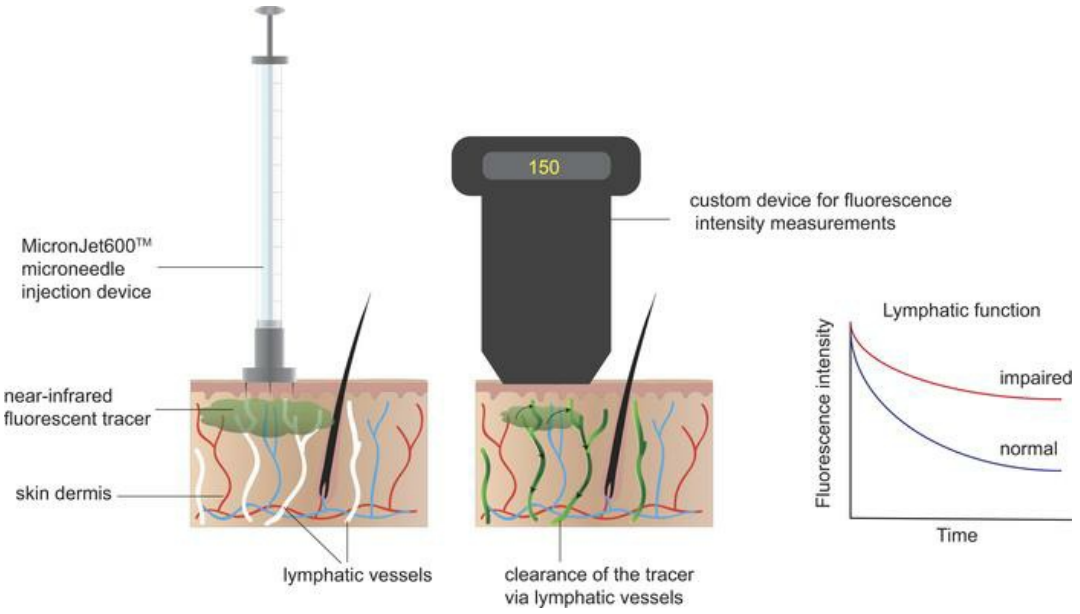

JCI insight

TECHNICAL ADVANCE

Minimally invasive method for the point-of-care quantification of lymphatic vessel function

Anna K. Polomska,[1] Steven T. Proulx,[1] Davide Brambilla,[2] Daniel Fehr,[3] Mathias Bonmarin,[3] Simon Brändli,[4] Mirko Meboldt,[4] Christian Steuer,[1] Tsvetina Vasileva,[1] Nils Reinke,[3] Jean-Christophe Leroux,[1] and Michael Detmar[1]

[1]Swiss Federal Institute of Technology (ETH Zürich), Institute of Pharmaceutical Sciences, Zürich, Switzerland. [2]University of Montreal, Faculty of Pharmacy, Montréal, Canada. [3]Zurich University of Applied Sciences, School of Engineering, Winterthur, Switzerland. [4]Swiss Federal Institute of Technology (ETH Zürich), Department of Mechanical and Process Engineering, Zürich, Switzerland.

Current clinical methods for the evaluation of lymphatic vessel function, crucial for early diagnosis and evaluation of treatment response of several pathological conditions, in particular of postsurgical lymphedema, are based on complex and mainly qualitative imaging techniques. To address this unmet medical need, we established a simple strategy for the painless and quantitative assessment of cutaneous lymphatic function. We prepared a lymphatic-specific tracer formulation, consisting of the clinically approved near-infrared fluorescent dye, indocyanine green, and the solubilizing surfactant Kolliphor HS15. The tracer was noninvasively delivered to the dermal layer of the skin using MicronJet600 hollow microneedles, and the fluorescence signal decay at the injection site was measured over time using a custom-made, portable detection device. The decay rate of fluorescence signal in the skin was used as a direct measure of lymphatic vessel drainage function. With this method, we could quantify impaired lymphatic clearance in transgenic mice lacking dermal lymphatics and distinguish distinct lymphatic clearance patterns in pigs in different body locations and under manual stimulus. Overall, this method has the potential for becoming a noninvasive and quantitative clinical "office test" for lymphatic function assessment.

Introduction

Lymphatic vasculature plays a vital role in maintaining tissue fluid homeostasis, immune surveillance, and the absorption of dietary fat in the intestine (1, 2). Alterations of lymphatic function have been associated with a number of diseases, including lymphedema (3), lipedema (4), venous insufficiencies (5), impaired wound healing (6), and chronic inflammatory diseases (7–9). Thus, reliable and reproducible techniques for the quantitative assessment of lymphatic vessel functionality are essential for diagnostic and monitoring purposes.

Advanced imaging techniques, such as computer tomography and magnetic resonance, have been used to qualitatively identify structural and functional changes of the lymphatic vasculature. However, these methods are not routinely applied in the clinics due to their complexity and associated high costs of instrumentation (10). The current "gold-standard" lymphoscintigraphy techniques are based on injection (subcutaneous, intradermal, or intramuscular) of radiolabeled colloidal particles or proteins that are specifically taken up by the lymphatic vasculature and allow for visualization of structural and functional abnormalities of lymphatic vessels (11–14). A method based on the injection of a radioactive tracer that is followed by monitoring of the decrease of the signal at the injection site over time (which represents the clearance of the tracer by the lymphatic vessels) can quantitatively reflect lymphatic vessel functionality (11, 12). However, the high costs of production and disposal, the environmental risks of radionuclides, the lack of standardization of the utilized colloids (^{99m}Tc-albumin used in Europe and ^{99m}Tc-sulphur in the US), the need for correcting the results due to radioactive decay, and the use of stationary and expensive scintigraphy cameras drastically hamper the widespread applicability of radioactivity-based methods.

Replacement of radioactive tracers with lymphatic-specific fluorescent dyes for lymphatic imaging and quantification eliminates the disadvantages of radioactivity and reduces the costs. In particular, tracers operating

Conflict of interest: The authors have declared that no conflict of interest exists.

Submitted: November 29, 2018
Accepted: January 14, 2019
Published: February 21, 2019

Reference information:
JCI Insight. 2019;4(4): e126515.
https://doi.org/10.1172/jci.insight.126515.

in the near-infrared (NIR) range, where optical absorption and scattering in biological tissues are low, allow for the acquisition of images with high-spatial resolution and with negligible background signals (15). In analogy to the quantitative scintigraphy-based methods, we and others have previously developed techniques for the quantitative measurement of lymphatic vessel drainage function that are based on monitoring the decay of the fluorescence signal after tissue injection of lymphatic-specific NIR fluorescent tracers in animal models (16, 17). However, these approaches rely on custom designed lymphatic-specific dyes or fluorescently labeled albumin, which are not approved for clinical use. Aqueous solutions of the only currently clinically approved NIR tracer, indocyanine green (ICG), are not suitable for this application due to aggregation and change of spectral properties of the dye after injection upon the monomerization caused by complexation with endogenous proteins (18, 19). This limitation might potentially be addressed by precomplexing ICG with nontoxic polymers, surfactants, or proteins that may prevent such interactions in vivo (20–23).

Another issue facing the use of NIR methods for lymphatic vessel function assessment, based on temporal measurements of the fluorescence signal of the locally injected probe, lies in the lack of suitable, affordable, and simple instrumentation for NIR fluorescence quantification for clinical use. Portable cameras (e.g., Hamamatsu PDE) would allow for quantitative imaging of ICG fluorescence in clinical settings by acquiring a series of images over time and quantifying the fluorescence signal based on image analysis (24, 25). However, the high cost of such instrumentation (ranging from several thousand up to tens of thousands of US dollars) limits their routine use outside specialized medical centers. Moreover, this type of measurement would be impractical due to the requirement for postmeasurement data processing (26–28). Therefore, the development of an affordable, compact, and portable fluorescence detector, without imaging capability but able to quantify the fluorescence signal intensity, would allow performance of the measurements in a routine manner outside of specialized hospital units (potentially even at a patient's home) (29).

A major challenge concerns the reproducible delivery of lymphatic-specific tracers to defined layers of the skin (12, 30). Due to the presence of a dense lymphatic plexus in the dermal layer of human skin, delivery of a NIR tracer directly to this layer would be most advantageous for the quantification of lymphatic vessel function (5, 12). However, intradermal injections, performed with conventional hypodermic needles, require special training of health professionals and are difficult to standardize (31). Potentially, this issue could be addressed by using microneedle-based injection systems that deliver molecules to a predetermined depth in the skin (31–33). Indeed, in our recent work, we developed 400- to 500-μm-long dissolving solid polymeric microneedles made of a mixture of poly(*N*-vinylpyrrolidone) (PVP) and ICG. After skin penetration, PVP dissolved and released ICG, allowing for quantitative assessment of lymphatic function in mice (20). Even though these studies identified an approach for quantitative imaging of lymphatic function, it was hampered by several limitations, such as challenging sterile manufacturing and upscale of production and the relatively the relatively low amount of tracer that could be delivered to the dermis (20).

In the present study, we pursued a three-pronged approach to develop an ICG-based tracer that can be administered intradermally via a microneedle-based injection device with hollow microneedles and a custom-designed portable NIR detection device for the quantitative assessment of lymphatic vessel function based on the clearance of the NIR tracer from the skin. This quantitative imaging method was validated in a genetic mouse model with impaired lymphatic vessel function in the skin and in pig studies with distinct lymphatic drainage. The minimal invasiveness of this method, together with the use of clinically approved tracer/excipient components and the compact quantitative signal detection device, provide great potential for the rapid clinical translation for the sensitive and early detection of impaired lymphatic vessel function.

Results

Physicochemical characterization of ICG-Kolliphor HS15 formulation. In aqueous solution, ICG forms H-aggregates, which monomerize upon interacting with endogenous proteins after injection. Since the spectral properties of ICG monomers are different from those of aggregates, (i.e., higher fluorescence intensity and bathochromic shift compared with aggregates), quantitative in vivo analysis of fluorescent signals from pure ICG-water is very challenging (19, 34–36). Therefore, it is preferable to have ICG in a stable monomeric form in the injected solution. To this end, we investigated the influence of several FDA-approved injectable solubilizing excipients (Supplemental Figure 1; supplemental material available online with this article; https://doi.org/10.1172/jci.insight.126515DS1) on the fluorescence intensity and emission maximum of ICG. The dye was mixed at a concentration of 0.05 mg/ml with solutions of the respective excipients at 100 mg/ml, and the fluorescence intensity and emission wavelength maximum were recorded. Among the tested

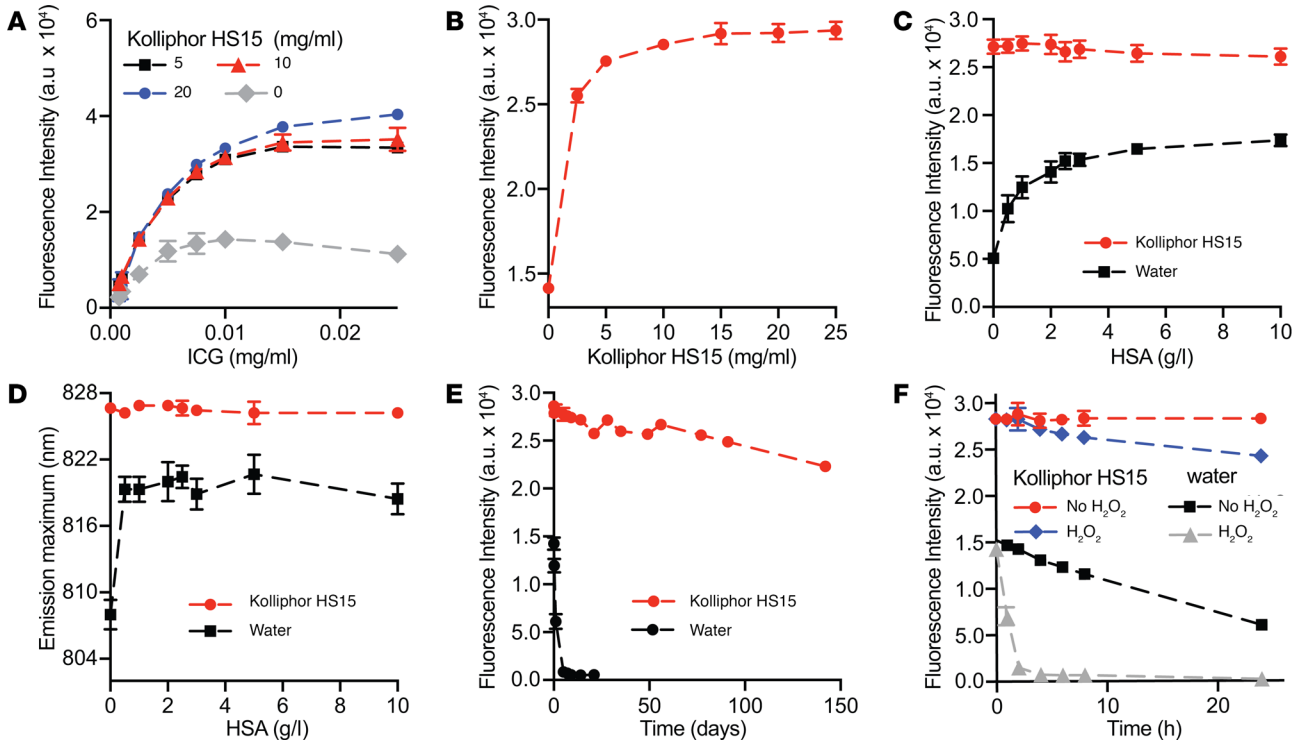

Figure 1. Influence of Kolliphor HS15 on spectroscopic properties of indocyanine green. If not otherwise stated, concentrations of indocyanine green (ICG) and Kolliphor HS15 were 0.0075 mg/ml and 10 mg/ml, respectively. (**A**) Fluorescence intensity of ICG at different concentrations in water or in Kolliphor HS15 solutions at 5, 10, and 20 mg/ml. (**B**) Fluorescence intensity of ICG in a solution containing Kolliphor HS15 at different concentrations. In **A** and **B**, fluorescence intensity is shown at 808 nm and 826 nm for ICG-water and ICG-Kolliphor HS15, respectively. (**C** and **D**) Influence of different amounts of HSA on spectroscopic properties of ICG-water and ICG-Kolliphor HS15. (**C**) Fluorescence intensity and (**D**) emission maximum of ICG-water and ICG-Kolliphor HS15 after mixing with HSA. Fluorescence intensity shown at 820 nm and 826 nm for ICG-water-HSA and for ICG-Kolliphor HS15, respectively. (**E** and **F**) Stability of ICG-water and in ICG-Kolliphor HS15. (**E**) Fluorescence intensity of the solutions measured over 140 days. Error bars are smaller than the symbols and not visible. (**F**) Fluorescence intensity of respective solutions measured over 24 hours in absence and in presence of 5 mM H_2O_2. In **E** and **F**, fluorescence intensity is shown at 808 nm and 826 nm for ICG-water and for ICG-Kolliphor HS15, respectively. Data presented in **A–D** and **F** were obtained in $n = 3$ individual experiments. Data in **E** were obtained in 1 experiment with 3 individual samples. All data are shown as mean ± SD.

excipients, Kolliphor HS15 (nonionic FDA- and EMA-approved surfactant, polyoxyl 15 hydroxystearate) and polysorbate 80 resulted in the highest increase in ICG fluorescence intensity (approximately 4-fold) and the largest bathochromic shift of the emission maximum (20 nm) (Supplemental Figure 1), in line with previously published data (37, 38). Since Kolliphor HS15 has been shown in preclinical studies to trigger an over 100-fold lower histamine release after i.v. injection compared with polysorbate 80 (39) and has not been found to cause anaphylactic reactions after parenteral application in humans (40), it was selected for further studies. When measured as a function of Kolliphor HS 15 concentration, the fluorescence intensity increase of ICG plateaued at 10 mg/ml (Figure 1, A and B), suggesting the full monomerization of the dye.

As previously mentioned, it is desired that ICG keeps identical spectral properties regardless of the presence of serum proteins (35). Because albumin is the most abundant serum protein in the body, we investigated the in vitro spectral properties of ICG in aqueous solutions and in Kolliphor HS15 in the presence of human serum albumin (HSA). Solutions of ICG-water or ICG in Kolliphor HS15 were mixed with solutions containing HSA at increasing concentrations. As seen in Figure 1, C and D, fluorescence intensity and emission maximum of ICG in Kolliphor HS15 formulation (ICG-Kolliphor HS15) were not affected by the HSA concentration. By contrast, the fluorescence intensity of ICG-water increased with increasing HSA concentrations in the solutions, and the emission maximum shifted from 808 nm to 820 nm, indicating dye monomerization. Together, these data show that Kolliphor HS15 is a good solubilizer for ICG that keeps the tracer in the monomeric state in solution.

Increased stability of ICG in Kolliphor HS15. ICG is known to rapidly degrade in aqueous solutions, resulting in a loss of fluorescence intensity (41, 42). Thus, we compared the stability of ICG in a pure aqueous solution to that of ICG in the presence of 10 mg/ml Kolliphor HS15 by measuring the fluorescence intensity

of the respective dye solution over time when stored at room temperature and protected from light. The fluorescence intensity of ICG in pure water was completely lost after 5 days, whereas for ICG-Kolliphor HS15, over 90% of the initial fluorescence intensity was retained after 60 days and 77% after 140 days (Figure 1E).

Qualitative LC-MS analysis of ICG-water incubated for 24 hours revealed the presence of a main ICG peak that eluted at 13.6 minutes (m/z = 753.42) and of a main degradation product at 12.09 minutes (m/z = 752.42) that could be assigned to an "irreversible" covalent dimer, as previously reported (42–44), as well as further smaller degradation products. In contrast, in ICG-Kolliphor HS15 solutions, the peak emerging from the plausible dimer was barely visible, even beyond 100 days after preparation (Supplemental Figures 2–4).

The increased stability of the ICG-Kolliphor HS15 may also have been due to a protective role of the encapsulation of the dye in the hydrophobic core of the surfactant micelles where the water-soluble oxidizing species have limited access, as previously suggested (37, 45, 46). To further investigate this phenomenon, we treated the ICG in water (ICG-water) and ICG-Kolliphor HS15 system with an oxidizing solution containing 5 mM H_2O_2. After 2 hours of incubation at room temperature, the fluorescence intensity of the ICG-water solution was completely lost, while the signal intensity of ICG-Kolliphor HS15 solutions was only reduced by approximately 10% after 24 hours (Figure 1F). We also investigated the stability of ICG in solutions containing PVP, as this polymer had been previously used in one of our former studies to deliver ICG with dissolving microneedles (20). In contrast to the previous study, we selected lower PVP concentrations that would result in lower solution viscosity, thus assuring injectability of the solution. As shown in Supplemental Figure 5, ICG was rapidly degraded in low-viscosity PVP solution, presumably due to presence of peroxide impurities in the PVP (47). Preincubation of PVP solutions with an antioxidant (i.e., sodium ascorbate) to inactivate the reactive oxygen peroxides (47, 48) improved the stability of ICG (Supplemental Figure 5). These results confirm the important role of oxidizing species in the degradation of ICG and a protective role of Kolliphor HS15 against them.

Efficient lymphatic clearance of injected ICG-Kolliphor HS15 formulations in mouse ears. We and others have previously shown that the clearance of an intradermally delivered lymphatic-specific tracer from an injection site correlates with the lymphatic drainage efficiency and can thus be used to quantify its function (16, 17, 20). ICG-water and ICG-Kolliphor HS15 (5, 10, and 20 mg/ml) were injected intradermally (3 μl each) into the ears of WT FVB mice, and the signal at the injection site was monitored over time with an IVIS in vivo imaging system. In ears injected with ICG-water, the signal was low and exhibited an initial increase phase up to 1 hour. However, for all ICG solutions containing Kolliphor HS15, a strong initial signal (10- to 14-fold higher than ICG-water) was recorded, followed by an exponential decay (Figure 2, A–C). After normalization to the initial value directly after injection, the signals from the ears injected with ICG-Kolliphor HS15 could be fit to curves of monoexponential decay with average R^2 values above 0.9 (Figure 2D). Half-lives calculated from the decay curves of ICG in Kolliphor HS15 at 5, 10, and 20 mg/ml were 4.0 ± 1.1, 3.6 ± 0.9, and 3.6 ± 0.6 hours, respectively, and were not significantly different from each other (Figure 2E).

We next investigated the perfusion of leg lymphatic vessels after intradermal administration of ICG (0.0075 mg/ml) in pure water and in the presence of Kolliphor HS15 (10 mg/ml). A bolus of 5 μl was intradermally injected in the dorsal aspect of the foot of the mice, and a stereomicroscope was used for visualization of the dye within draining lymphatic vessels of the lower hindlimb. For both solutions, the dye could be seen within the collecting lymphatic vessels. Applying external compression at the injection site after injection of ICG-Kolliphor HS15 solution stimulated further uptake of the dye only into the lymphatic vessels, in contrast to ICG-water, which could also be visualized in the draining popliteal vein (Supplemental Figure 6, A–C).

Next, we investigated the potential of the ICG-Kolliphor HS15 formulation to quantify lymphatic clearance in a previously validated mouse model of reduced lymphatic function (49). To this end, we employed transgenic K14-VEGFR3-Fc mice, which express a soluble vascular endothelial growth receptor-3 that scavenges vascular endothelial growth factors C and D (VEGF-C and VEGF-D), resulting in impaired development of dermal lymphatic vessels (17, 49). A bolus of 3 μl of the formulation was intradermally injected into both ears of K14-VEGFR3-Fc–transgenic and WT control mice, and the signal was monitored over time with the IVIS imaging system. In both mouse lines, the normalized signals over time exhibited a close fit to a one-exponential decay function (Figure 3A). As expected, the lymphatic clearance was significantly slower in the K14-VEGFR3-Fc–transgenic mice than in WT mice (half-lives, 9.6 ± 1.8 hours vs. 2.6 ± 0.8 hours, respectively, $P < 0.001$) (Figure 3B). Together, these results indicate that the ICG-Kolliphor HS15 formulation can be used for quantitative assessment of lymphatic clearance.

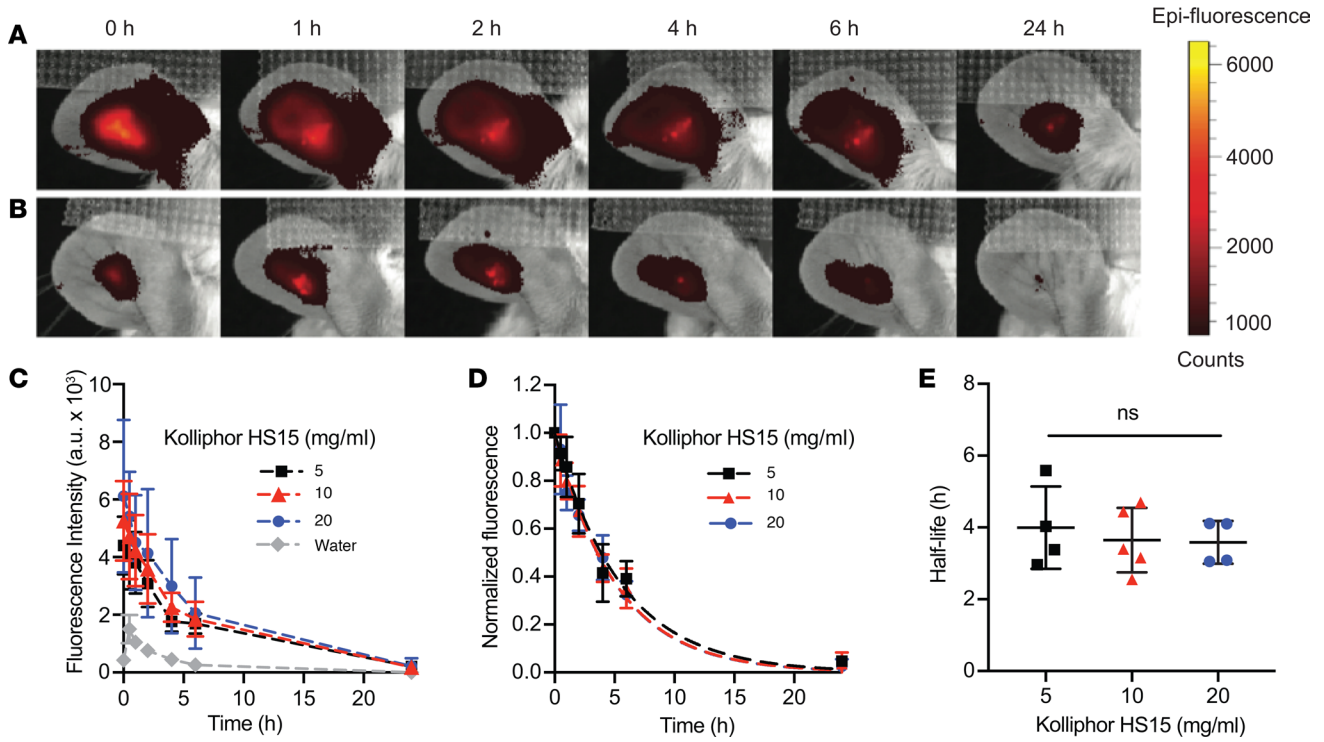

Figure 2. Clearance kinetics after bolus intradermal administration of indocyanine green in water or in a solution of Kolliphor HS15 into mouse ears. If not otherwise stated, the concentrations of indocyanine green (ICG) and Kolliphor HS15 in the solutions were 0.0075 mg/ml and 10 mg/ml, respectively. (**A** and **B**) Representative IVIS images of fluorescence signal dynamics in mouse ears after intradermal injection of 3 μl ICG in (**A**) a solution of Kolliphor HS15 and (**B**) water. (**C**) Quantification of fluorescence signal intensity in mouse ears over time after injection of ICG-water and ICG-Kolliphor HS15 solutions. (**D**) Normalized fluorescence intensity over time for mouse ears injected with ICG-water and ICG-Kolliphor HS15 and fitting of monoexponential decay curves (represented by lines). (**E**) Quantification of dermal elimination half-life calculated from fitted curves. For **C** and **D**, data are presented as mean ± SD (n = 3 per group for ICG-water and n = 4, 5, and 4 for 5, 10, and 20 mg/ml ICG-Kolliphor HS15, respectively, where n represents an ear). For **E**, the data were compared by 1-way ANOVA with Tukey's multiple comparison post hoc analysis; ns, $P \geq 0.05$.

Design and in vitro validation of a portable NIR fluorescence detection device. Portable NIR cameras are often used for clinical imaging purposes and could be suitable for signal quantification. However, the measurements would be limited to specialized medical centers due to the high prices of such instrumentation (24, 50). Therefore, we next built a prototype system for the simple and inexpensive quantitative fluorescence detection of injected NIR tracers. This device is portable and therefore would be particularly suited for the clinical monitoring of lymphatic clearance of NIR probes outside of the hospital (e.g., at the local general practitioner or at a patient's home) (Figure 4A, Supplemental Figure 7, and Supplemental Text).

A linear relationship between dye concentration (in 10 mg/ml Kolliphor HS15) and fluorescence intensity with the device was confirmed in vitro (Figure 4B). The intraday variability and repeatability of the measurements was assessed by measuring the ICG solutions 5 times. For interday repeatability, the same solutions were measured over 3 days. The results demonstrated a very good intraday and interday repeatability of the signal for all measured concentrations, as reflected by low values of coefficient of variations (%COV below 6% for intraday variability and below 15% for interday variability) (Supplemental Tables 1 and 2).

Portable device measurements in awake versus anesthetized mice. Since it is not possible to perform measurements with the portable device on the small surface area of mouse ears, we initially aimed to validate the device in the back skin of mice. A bolus of 5 μl of the ICG-Kolliphor HS15 was injected intradermally, and the signal at the injection site was measured over time with both the IVIS imaging system and our device prototype. The diameter of the region of interest (ROI) analyzed by IVIS was set to 3 cm (Figure 5, A and B, blue circle) similar to the diameter of the region analyzed by the device (Figure 5, A and B). Since the lymphatic transport is reduced in anesthetized mice (51), as compared with awake mice, we first tested whether we could detect a difference in lymphatic clearance between those two conditions. Therefore, one group of mice was kept continuously anesthetized with isoflurane between the imaging sessions, and the second group was awake and anesthetized shortly only for the measurements. In contrast to our findings

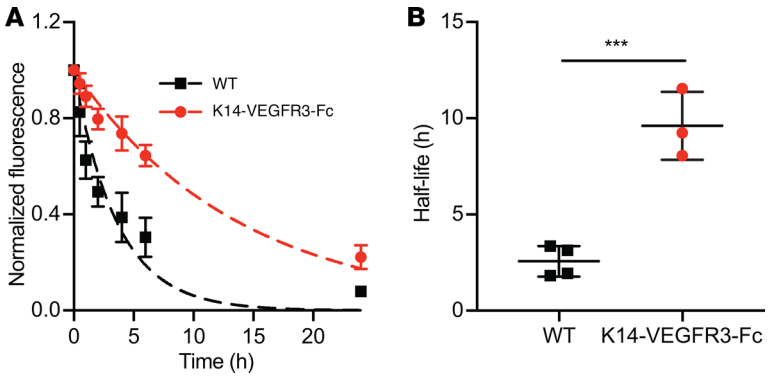

Figure 3. Quantification of dermal lymphatic drainage after bolus intradermal administration of 3 μl indocyanine green (0.0075 mg/ml) in Kolliphor HS15 (10 mg/ml) into the ears of WT and K14-VEFGR3-Fc mice lacking a dermal lymphatic vasculature. (**A**) Normalized fluorescence intensity over time and fitting of monoexponential decay function in WT (n = 4 mice per group) and K14-VEGFR3-Fc (n = 3 mice per group) mice. (**B**) Quantification of dermal elimination half-lives in WT and K14-VEFGR3-Fc mice from fitted curves. For **B**, data were compared by Student's t test; ***$P < 0.001$. ICG, indocyanine green.

after tracer injection into mouse ears, where the signal exhibited immediate decay, the average fluorescence signal intensity in the back skin of awake mice, measured by IVIS, slightly increased in the first hour (approximately 1.1-fold). This is likely due to diffusion of the dye in the tissue and/or distribution to initial lymphatics prior to the lymphatic clearance phase (signal decrease) (5, 11–13, 16, 52). In anesthetized mice, the signal intensity slowly increased around 1.3-fold for up to 3 hours, followed by a slow decrease in signal over time. With the portable device, the decrease of the signal was observed already at 1 hour in the awake group and at 2 hours in the anesthetized group (Figure 5C).

Since fitting using a monoexponential decay function and half-life calculation were not possible, we used an AUC of the normalized clearance curves to assess the total tissue clearance of the tracer from the injection site. The AUCs calculated for curves obtained with the device were slightly lower than those obtained with the IVIS, but the values obtained with either method were not statistically different from one another. Importantly, for both measurement methods, the differences in average AUCs for awake and anesthetized groups were highly significant (IVIS anesthetized, 6.9 ± 1.1 hours; IVIS awake, 4.9 ± 0.3 hours; device anesthetized, 6.1 ± 0.8 hours; device awake, 4.0 ± 0.5 hours; $P < 0.05$ between IVIS anesthetized and IVIS awake; $P < 0.01$ between device anesthetized and device awake) (Figure 5D). Moreover, a significant correlation between the AUCs calculated from the IVIS measurements and from the portable device measurements was found (Pearson's correlation coefficient $r = 0.9475$, $P < 0.001$) (Figure 5E).

In conclusion, the portable device was able to distinguish differences in tissue clearance in vivo with close agreement to standard imaging methods.

Validation of portable device measurements in pigs. Pig skin exhibits structural and functional resemblance to human skin, with the thickness of the pig and human epidermis varying from 30 to 140 μm and 50 to 120 μm, respectively, depending on the anatomical location and age (53–55). We used three 1-month-old female domestic pigs (10–14 kg), which are more suited for handling (i.e., easy for manual restraint under awake conditions). Injections were performed on the ventral aspect of the torso of the animals due to the large area accessible for injection as well as the thinner (56) and visually less keratinized skin compared with the rest of the body, enabling facile penetration of microneedles through the skin. The ICG-Kolliphor HS15 formulation was administered using MicronJet600 microneedles (3 pyramid-shaped microneedles, each 600 μm long), enabling standardized and uniform delivery of the tracer formulation through the epithelium directly to the dermal skin layer (57).

In pig 1, we investigated the effect of manual compression of the injection site on the tissue clearance from the skin under anesthesia. Similar to muscular activity, manual compression promotes the entrance of interstitial fluid into the initial lymphatic capillaries and thus increases lymphatic clearance (51, 58). Four symmetrical intradermal injections (Figure 6A) of ICG-Kolliphor HS15 (50 μl) were performed on the left and right part of the ventral aspect of the torso, and the injection sites on the right site were manually massaged with a circular motion using fingers throughout the whole duration of the experiment (except for

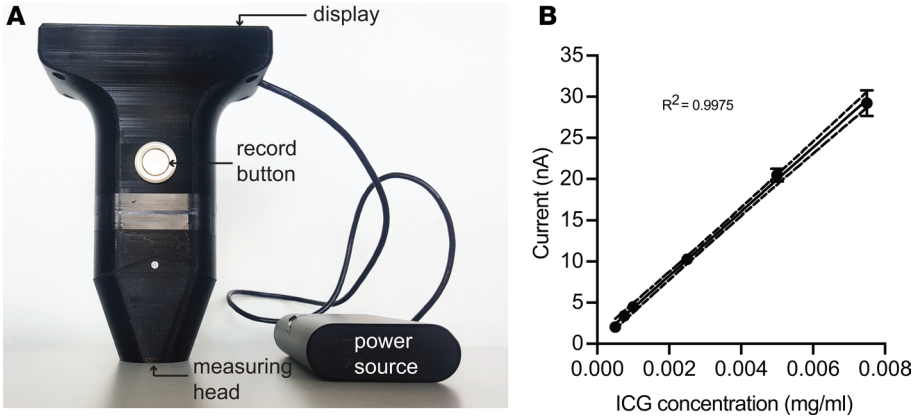

Figure 4. Custom portable device for near-infrared fluorescence measurements used in this work. (**A**) Set-up of the device. After placing the measuring head over the sample, the values (in nA units) are recorded by pressing the button on the side of the device and are shown on the display. The device operates with an external power source. (**B**) In vitro calibration curve with 95% confidence intervals (dashed lines) obtained with the device for ICG solutions at different concentrations in Kolliphor HS15 (10 mg/ml). Data are presented as mean ± SD, *n* = 5. ICG, indocyanine green.

during the measurements). The fluorescence signal at the injection site was measured every 30 minutes with the portable device (Figure 6B). Eight to eleven measurements at the same injection site were performed by lifting the device between each measurement. Supplemental Table 3 shows the average fluorescence values obtained from all measurements, together with the exact number of readings per injection site (*n*), SD, and relative SD (RSD%) obtained in pig 1. There was slight variability between the measurement; however, the %RSD never exceeded 15 %. The variability arose from the difficulty in selecting the same location for each reading. Therefore, only the 3 highest values were used for further data analysis, which leads to an assumption that the same location was always selected at every time point.

Normalized clearance curves obtained for each injection site are shown in Figure 6, C and D. For 3 of 4 nonmassaged injection sites, a very slow signal decrease was observed, whereas for most of the massaged injection sites, the fluorescence intensity already decreased after 1 hour. We calculated AUCs to estimate the overall tissue clearance from the injection sites (Figure 6E). On average, applying the compression on the contralateral sites decreased the AUC from 1.2- to 1.5-fold. A paired analysis of the AUCs from the nonmassaged and massaged sites produced a highly significant statistical difference between the two groups (average AUC from nonmassaged sites, 3.4 ± 0.4 hours; average AUCs from massaged sites, 2.5 ± 0.5 hours; $P < 0.01$).

Validation of the portable device for tissue clearance measurements in awake pigs. In pig 1 (Figure 6), we observed a trend of rapid tissue clearance in the pectoral region that was reduced in the pelvic area that may emerge from regional tissue properties and lymphatic vessel density differences. Thus, we next investigated the tissue clearance in two awake pigs (pigs 2 and 3) at different locations of the ventral torso (Figure 7, A and C). In pig 2, the fastest tissue clearance occurred in the pectoral region, as evidenced by the lowest AUCs (2.3 and 2.4 hours). For the injections in the middle part of the torso, the calculated AUCs increased to around 3.0 hours. The highest AUC values were found in the pelvic area of the torso (3.6 and 3.7 hours) (Figure 7B). A similar trend was found in pig 3; however, a slower tissue clearance was found in the middle part of the torso than in pig 2 (Table 1 and Figure 7D). The pooled AUCs from all 3 areas (pectoral, middle torso, and pelvic) from both pigs are shown in Figure 7E. The statistical differences between AUCs at different injection sites were highly significant. In conclusion, the portable device in combination with the ICG formulation delivered via microneedles reliably distinguished different lymphatic vessel clearance patterns in pig skin.

Discussion

In this study, we established a simple method for the quantitative assessment of lymphatic vessel function in the skin, based on tracking of the disappearance of the fluorescence signal of a lymphatic-specific NIR tracer system containing ICG using a custom-made portable detection device after injection of the tracer with hollow microneedles into the dermis. The successful validation of this method in

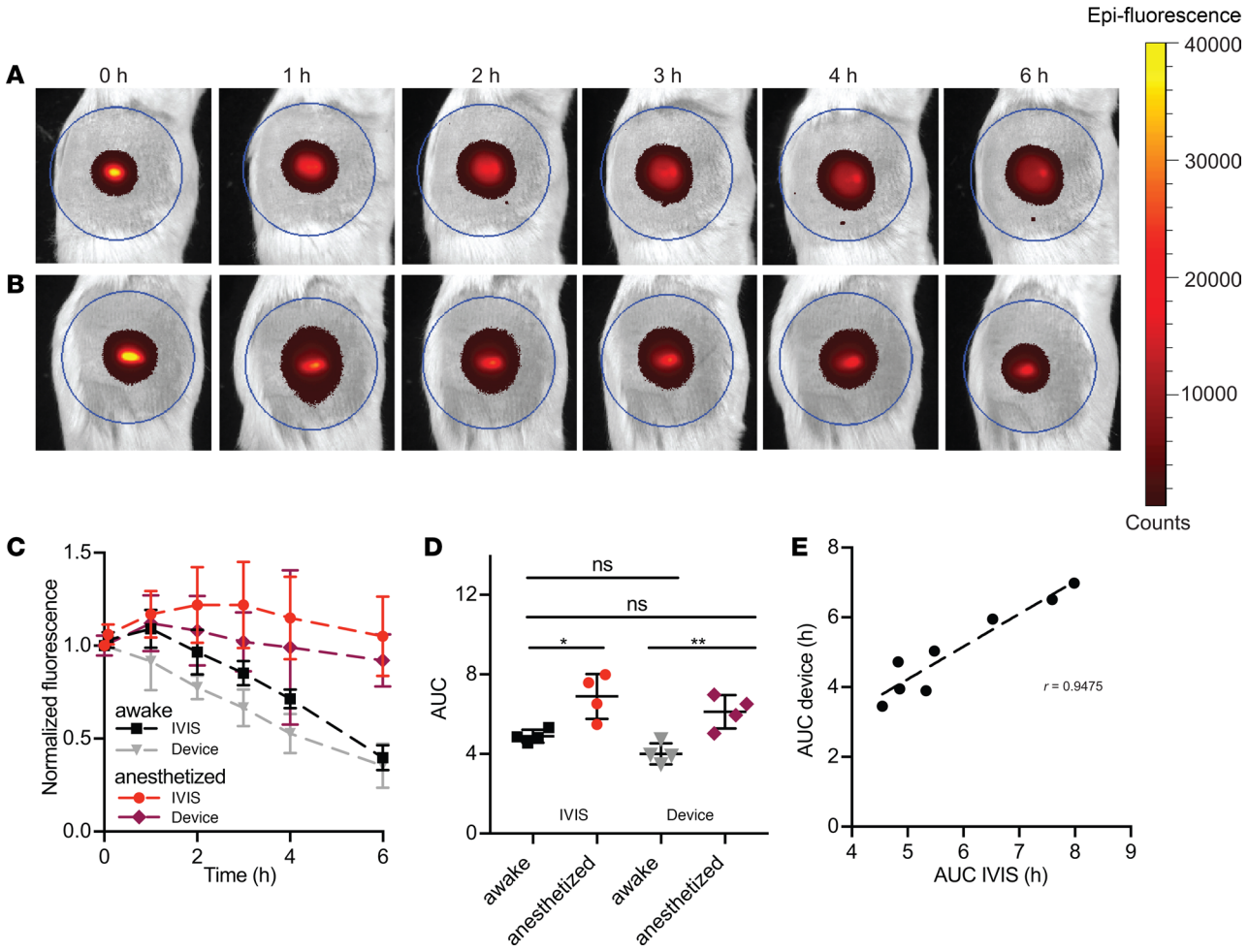

Figure 5. Clearance kinetics after bolus intradermal administration of 5 μl of the solution of indocyanine green (0.0075 mg/ml) in Kolliphor HS15 (10 mg/ml) into the back skin of WT mice. Representative IVIS images of fluorescence signal dynamics in the skin of (**A**) an anesthetized and (**B**) an awake mouse. (**C**) Dynamics of normalized fluorescence signal in the back skin of awake and anesthetized mice obtained with IVIS and the device. Data are presented as mean ± SD, $n = 4$ mice for the awake and anesthetized group. (**D**) Quantification of the normalized clearance curves obtained with IVIS and the device in anesthetized and awake mice by AUC. Data are presented as mean ± SD and compared with 1-way ANOVA with Tukey's multiple comparison post hoc analysis; $^{*}P < 0.05$, $^{**}P < 0.01$. (**E**) Correlation between AUCs obtained by measuring the signal with the use of IVIS and the device. ICG, indocyanine green; *r*, Pearson's correlation coefficient.

mice and young pigs supports its potential utility for simple and reliable quantifications of lymphatic clearance in clinical settings.

The first component of the method is an improved ICG formulation that includes a surfactant, Kolliphor HS15, encapsulating dye molecules in the hydrophobic micellar core. This overcomes major limitations associated with the use of purely aqueous solutions of this clinically approved tracer for lymphatic clearance assays. In aqueous solutions, ICG aggregates, which leads to strong fluorescence self-quenching, resulting in a nonlinear concentration-fluorescence intensity dependence as well as blue shifts in absorption and emission maxima compared with the monomeric form (41). After injection of purely aqueous ICG solutions, the dye monomerizes upon interaction with endogenous proteins (i.e., albumin and lipoproteins), which results in an increase in fluorescence intensity and red shifts in the emission and absorption maxima (20), both of which complicate quantitative analyses over time. To address this issue, ICG should ideally be administered in a monomeric form. With the ICG-Kolliphor HS15 combination, the fluorescence intensity and wavelength of maximum emission (826 nm) remained unchanged upon adding HSA, in contrast to purely aqueous ICG solutions. These results suggest that, after intradermal injection of ICG in Kolliphor HS15, the majority of the tracer would remain bound to the surfactant and remain in the micellar core in a monomeric state.

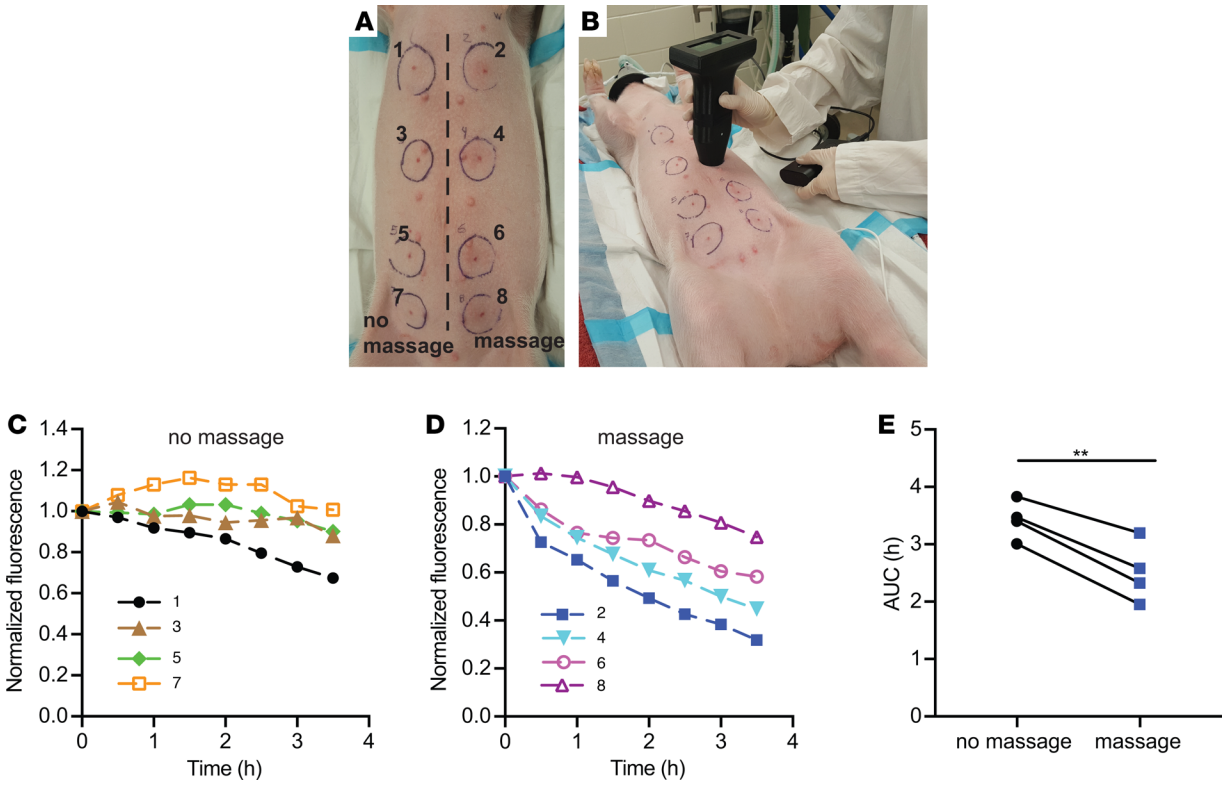

Figure 6. The effect of manual stimulation on lymphatic clearance in the ventral aspect of the torso of anesthetized pig 1 after bolus intradermal administration of 50 μl indocyanine green (0.0075 mg/ml) in a solution of Kolliphor HS15 (10 mg/ml) using MicronJet600 microneedles. (**A**) Injection pattern, indicating labeling of the injection and massaged sites. (**B**) Measurements of the fluorescence signal with the use of the device. (**C** and **D**) Normalized fluorescence signal at each injection site over time in (**C**) nonmassaged and (**D**) massaged sites. (**E**) AUCs of ICG clearance curves from paired nonmassaged and massaged sites and comparison of sites 1 and 2 from the chest region. *n* represents the number of injection sites, and *n* = 4 for massaged and nonmassaged sites. Data were compared by paired Student's *t* test; $^{**}P < 0.01$. ICG, indocyanine green.

These findings were validated in vivo, where the injection of ICG in pure water into mouse ears resulted in a very low initial fluorescence signal that was followed by an almost 10-fold increase after 1 hour, likely due to interactions with endogenous proteins. By contrast, the initial signal after administration of ICG-Kolliphor HS15 in a concentration range of 5–20 mg/ml was more than 20-fold higher compared with ICG-water. This is in agreement with a recent publication where a stronger signal intensity of ICG-Kolliphor HS15 in retinal vasculature in vivo was found compared with ICG in pure water (38). Encapsulation of ICG in Kolliphor HS15 micelles also significantly improved the chemical stability of the dye compared with purely aqueous solutions, in agreement with a previous study (37).

The second important part of this work is the development of an inexpensive, compact, and portable system for NIR fluorescence detection in the skin, enabling fluorescence signal intensity measurements without the need for imaging capabilities. Due to its small size, external power source, and incorporated display, the device could be easily operated at any location, e.g., in different animal facilities and in different animal species (i.e., mice and pigs) as well as in humans.

The third component of the clearance assay is the use of a microneedle-based injection device, MicronJet600, that enables the painless, uniform delivery of a tracer to a controlled depth in the skin (to around 600 μm) (57). The importance of a homogenous injection depth for the reproducibility of clearance assays has been highlighted in previous studies using radioactive tracers (5, 12, 30).

To apply a correct mathematical model for analyzing the lymphatic clearance curves, one should keep in mind that various clearance patterns can be measured in the skin in different body parts in vivo. For example, the clearance patterns of ICG in Kolliphor HS15 in the back skin of the mouse and in the pig torso differed from those obtained in mouse ears. In mouse ears, the signal always followed a monoexponential-like decay over time. Therefore, the ICG removal from the injection site could be easily quantified by computing the signal half-life from normalized experimental data. The dermal elimination half-lives in

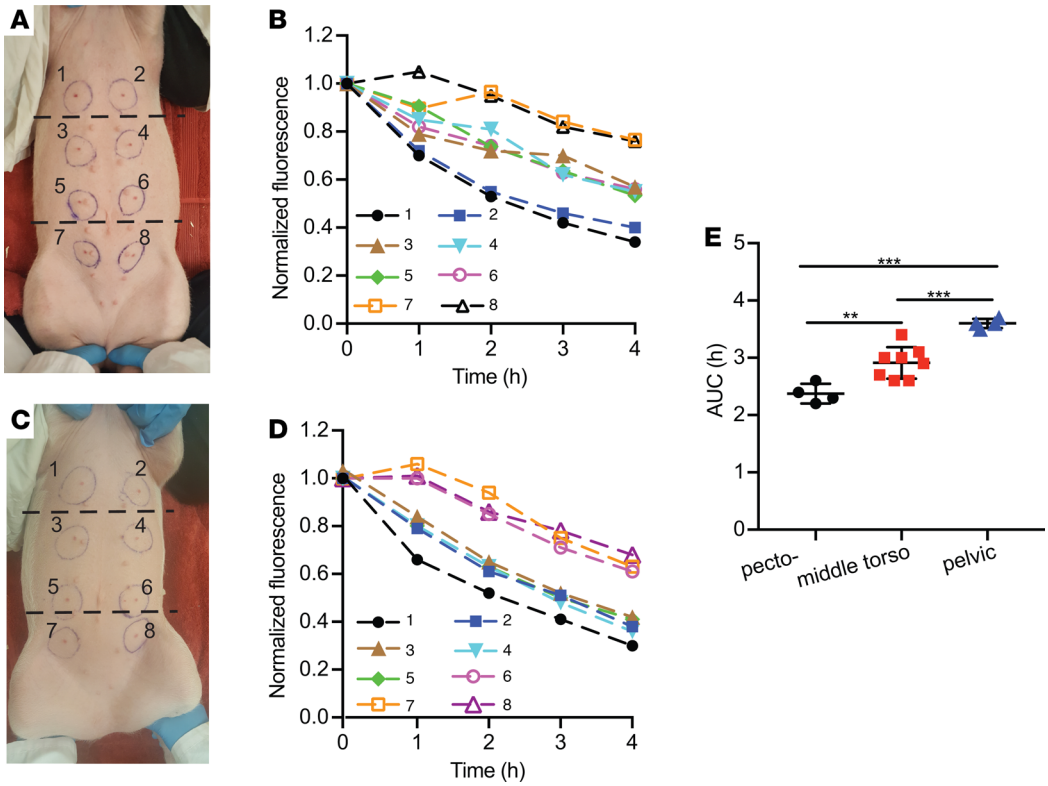

Figure 7. Lymphatic clearance from the skin at the ventral aspect of the torso of awake pigs after bolus intradermal injection of 50 μl indocyanine green (0.0075 mg/ml) in a solution of Kolliphor HS15 (10 mg/ml) with the use of MicronJet600 microneedles. (**A**) Injection sites in pig 2. (**B**) Normalized fluorescence signal at each injection site over time in pig 2. (**C**) Injection sites in pig 3. (**D**) Normalized fluorescence signal at each injection site over time in pig 3. (**E**) AUCs of the clearance curves from the pectoral, middle torso, and pelvic area. *n* represents the number of injection sites at different locations in the abdomen in 2 pigs, and *n* = 4 for pectoral, *n* = 8 for middle torso, and *n* = 4 for pelvic site. Data are presented as mean ± SD and compared with 1-way ANOVA with Tukey's multiple comparison post hoc analysis; $^{**}P < 0.01$, $^{***}P < 0.001$.

transgenic mice lacking a dermal lymphatic vasculature (K14-VEGFR3-Fc–transgenic mice) were on average 4-fold higher than those in WT mice, which agrees well with the previous data (17).

In contrast, in the back skin of mice, the fluorescence signals typically started to decrease only 1 or 3 hours after injection (in awake and anesthetized mice, respectively), and this was preceded by a 10% intensity increase. Similarly, in some locations of the pig torso, the fluorescence signal decreased only after around 1 hour after injection. Such a lag phase with no or very little clearance can most likely be attributed to the tracer diffusion into the tissue, prior to entering the initial lymphatic capillaries. This phenomenon has indeed been described in several studies with both radioactive and fluorescent probes (5, 11–13, 16). Modi et al. (59) reported an initial increase of the counts of subcutaneously injected radioactive IgG prior to the decrease phase, suggesting transport of the probe to more superficial layers of the skin, which could also be the case in our experiments. The absence of the signal increase phase in ear skin is likely related to the lower tissue compliance compared with mouse back skin and to some locations in the pig torso. A low tissue compliance could create a more favorable interstitial pressure gradient after injection, thus promoting fluid (and tracer) uptake by the lymphatic vessels (60, 61). The lack of an immediate signal decrease can obviously complicate the calculation of the dermal elimination half-life of ICG. Previously, this problem has been addressed by fitting the exponential function starting from a later time point when the signal starts to decay (5, 11–13, 16, 52). However, the time point when the signal begins to decrease may vary. It could be different in healthy and in lymphedematous extremities of patients or it might change with disease progression. A longer diffusion phase could also be expected in lymphedema. To address these issues, we indirectly assessed lymphatic tracer clearance by calculating the AUC area under the normalized clearance curve, taking into account the tracer diffusion phase. Our current efforts are directed toward replacing a

Table 1. AUCs of the respective curves from Figure 7, B and D

Injection number	Injection site	AUC (h)	
		Pig 2	Pig 3
1	Pectoral	2.3	2.2
2		2.4	2.6
3	Middle torso	2.9	2.7
4		3.1	2.6
5		3.0	2.6
6		3.0	3.4
7	Pelvic	3.6	3.6
8		3.7	3.5

simple AUC analysis with a more sophisticated mathematical model that would describe both diffusion in the skin and lymphatic clearance.

The AUC quantification method was successfully applied to analyze the results of the clearance assays in pigs. Since manual therapy is often applied as a treatment in lymphedema patients to stimulate lymphatic clearance, we investigated the effect of manual compression on lymphatic clearance of the NIR tracer from the skin in an anesthetized pig. Our findings that the clearance from the massaged injection sites was improved, as reflected by a 1.3-fold lower AUC, are in agreement with previous studies by Mortimer et al. where the half-life of clearance of ^{99m}Tc-colloid was almost 2-fold enhanced in massaged sites in pigs (12).

The fact that we observed faster lymphatic tracer clearance from the skin of awake pigs in the pectoral torso area than in the middle torso or pelvic area is likely due to the breathing motions in the pectoral area that stimulate uptake of the tracer by initial lymphatics and to differences of the skin structure, tissue compliance, and density of the lymphatic vasculature (60, 61). Our findings are in agreement with previous studies of lymph flow variations between different body parts in animals and humans (12, 59, 62) and indicate the importance of selecting comparable locations for tracer injections if clearance data are compared over time (e.g., during disease progression) or between healthy and lymphedematous extremities.

Our method for assessing lymphatic function presents a number of advantages over existing techniques. It is minimally invasive as the solution is intradermally injected with microneedles, a procedure that is simple and painless. The components of the formulation (i.e., Kolliphor HS15 and ICG) are approved for parenteral administration and the portable device can be produced at a relatively low cost and does not require any specialized facilities, potentially allowing a rapid progression in the clinic. This device must, however, be placed at the same area of the skin for each single measurement, potentially creating variability due to small shifts of the measured area. Therefore, our current efforts are directed toward the development of a miniaturized, wearable detection device that can be attached to the skin. This would enable the continuous monitoring of NIR fluorescence signals over several hours, shortening the measurement time period and allowing for more complex analyses that might better reflect the ratio between diffusion and clearance (e.g., by determining the time needed to reach the maximum fluorescence signal intensity). These improvements could facilitate a more precise quantification of lymphatic function under normal and pathological conditions.

Methods

Chemicals. VERDYE, a clinical-grade ICG (Diagnostic Green GmbH) was used in this study. ICG aliquots were prepared by dissolving the dye in anhydrous methanol, preparing small portions, and evaporating the solvent under a stream of nitrogen. Kolliphor HS15 and PVP (Kollidon 12 PF), injectable grades, were purchased from BASF. Sodium ascorbate (USP grade) was from AppliChem. γ-Cyclodextrin was purchased from Wacker, sodium deoxycholate was purchased from ABCR, and TPGS was purchased from BASF. HSA (≥90%, recombinant) was obtained from MilliporeSigma, and H_2O_2 (35%, stabilized, for analysis) was purchased from Acros Organics. Ultrapure water from Nanopure Diamond Barnstead system (Thermo Scientific) was used.

Animals. Mice were kept under specific pathogen–free conditions until imaging. FVB mice were bred in-house, and K14-VEGFR3-Fc–transgenic mice were provided by Kari Alitalo, University of Helsinki,

Helsinki, Finland (17, 49). Three 4-week-old female domestic pigs (10–14 kg) were obtained from local Canadian farmers. Prior to starting any procedures, the animals were acclimatized for 1 week in the facility.

Spectroscopic measurements. ICG solutions were prepared by dissolving dye aliquots in water or in a solution containing the respective solubilizer. Fresh solutions were always prepared and used the same day. Spectra were recorded on a plate reader (Tecan Infinite M200 Pro, Tecan GmbH). Fluorescence measurements were performed using Costar 96-well, black, flat-bottom plates (Corning Inc.). Briefly, 200 µl of the solutions was pipetted into the well, and the fluorescence intensity was measured using the following settings: $\lambda_{ex}/\lambda_{em}$ = 700/750–850 nm, gain: 125. Experiments were performed in triplicates.

Surfactant screening study. We investigated the influence of several FDA-approved injectable synthetic and bioderived solubilizing excipients (Kolliphor HS15, polysorbate 80, sodium deoxycholate, Poloxamer188, γ-cyclodextrin, d-α-tocopherol polyethylene glycol 1000 succinate [TPGS], and PVP) on the fluorescence intensity and emission maximum of ICG. Briefly, 0.5 ml ICG dissolved in water at a concentration of 0.05 mg/ml was mixed with equal volumes of solutions of the respective excipients at 100 mg/ml, and the fluorescence intensity and emission maximum were recorded using a plate reader as described above.

Stability studies. In all stability experiments, the fluorescence intensity of the solutions was measured over time using a plate reader as described above. The solutions were stored at room temperature and were protected from light. For H_2O_2-induced degradation studies, 0.75 ml of ICG solutions (0.015 mg/ml) in Ultrapure water or in Kolliphor HS15 (20 mg/ml) were diluted with equal volumes of Ultrapure water containing 10 mM H_2O_2. The fluorescence intensity of the resulting solutions was measured over time as described above. The solutions were stored in the dark at room temperature, and experiments were performed in triplicates.

Interactions with albumin. The fluorescence intensities of ICG-water and ICG-Kolliphor HS15 solutions in the presence of HSA were measured using a plate reader. Briefly, 0.75 ml of solutions of ICG (0.015 mg/ml) in Ultrapure water or in Kolliphor HS15 (20 mg/ml) were diluted with equal volumes of 2× PBS at pH 7.4, containing increasing concentrations of HSA. Experiments were performed in triplicates.

LC-MS analyses. All samples were analyzed using a LTQ/XL/ETD linear ion trap (Thermo Scientific) mass spectrometer coupled to a Waters Acquity UPLC. Gradient elution was done on a Waters XBridge C18 column (3.0 × 150 mm, 3.5 µm). The mobile phase consisted of 10 mM aqueous ammonium formate plus 0.1% formic acid (eluent A) and 90% acetonitrile in ammonium formate (final 10 mM) plus 0.1% formic acid (eluent B). The flow rate was set to 0.3 ml/min, and the gradient was programmed as follows: 0–1 minutes 5% B, 1–20 minutes to 100% B, 20–22 minutes 100% B, 22–22.1 minutes to 5% B, 22.1–25 minutes 5% B. The column oven and the autosampler were set to 30°C and 10°C, respectively. The injection volume for all samples was 10 µl. Between each sample a blank injection (water) was programmed, accounting for possible carry over due to PVP and ICG. MS settings were used as reported by Wissenbach et al. (63). The MS was equipped with heated ESI II source was set to 200°C. All measurements were performed in the positive ionization mode.

The following samples were analyzed by LC-MS (in triplicates): fresh solutions of ICG (0.0075 mg/ml) in water and in 10 mg/ml Kolliphor HS15, the same samples stored for 24 hours, and aged solutions of ICG–Kolliphor HS15 (106 days). All solutions were stored at room temperature and were protected from light.

Lymphatic clearance assay in mouse ears. An IVIS Spectrum (Xenogen, Caliper Life Sciences) imaging system was used for the in vivo lymphatic clearance assay. 10- to 12-week-old male mice were used for the assays (FVB or K14-VEGFR3-Fc [transgenic or WT]). Detailed protocols for this assay are described elsewhere (17, 20, 64). Briefly, mice under 2% isoflurane anesthesia were injected intradermally in the ears with 3 µl of a freshly prepared solution containing ICG (0.0075 mg/ml if not otherwise stated) in water or in a Kolliphor HS15 solution using 29-gauge insulin syringes (Terumo). The fluorescence signal in the ears was monitored at predetermined time points (0, 1, 2, 4, 6, and 24 hours). Measurements were performed in isoflurane-anesthetized mice, but between the measurements the animals were allowed to move without any restriction. The signal was measured using the following settings: $\lambda_{ex}/\lambda_{em}$ = 745/800 nm, exposure time: 1.5 or 2 seconds, small binning, field of view: 6.6 cm × 6.6 cm. The images were analyzed by drawing the ROI around the administration site, and the average fluorescence intensity was measured for each time point using Living Image Software (Caliper Life Sciences). After subtracting the background signals, the values were normalized to the time 0 measurement and plotted against time. A monoexponential decay function was fitted to the obtained data, and the dermal elimination half-lives were calculated using GraphPad Prism 7 software (constrain parameters for fitted curve: at time 0 hours, the value is equal to 1, the plateau value is 0).

Portable fluorescence detection device. The portable hand-held device for NIR fluorescence quantification was custom-made for this application. The device was equipped with an external power supply and has a circular field of view with an inner diameter of 3 cm. The optical components are enclosed into a custom-designed 3D-printed case made of black-colored poly(lactic acid). The optical set-up (Supplemental Figure 7, A and B) consists of two 785-nm laser diodes that are placed opposite to each other and serve as excitation sources. Each laser diode illuminates the surface at an angle of 60. The fluorescent light emitted by the ICG after laser illumination passes through a custom optical set-up, consisting of a pinhole and 2 lenses and a long-pass filter with a cutoff at 820 nm. The filtered light reaches a photodiode detector that generates photocurrent proportional to the incident light intensity. The photocurrent is acquired by the device's electronic and control algorithm and was finally shown to the user as a current reading in nA (Supplemental Figure 7C). More information about the device can be found in the Supplemental Text.

For in vitro validation of the device, a series of ICG solutions (0.0075–0.00075 mg/ml) in Kolliphor HS15 (10 mg/ml) were prepared. Briefly, 0.5 ml of the solution was placed in a well of a 6-well plate (TPP, MilliporeSigma) protected from light by black isolation tape, and the fluorescence intensity was measured with the device. The intraday repeatability of the measurements was assessed by measuring the ICG fluorescence intensity 5 times in the same well. For interday repeatability, the same solutions were used over 3 days.

Lymphatic clearance assay in the back skin of anesthetized and awake mice. The IVIS Spectrum imaging system and the custom portable device were used simultaneously for the in vivo clearance assay in the back skin of mice. Eight 19-week-old male FVB mice were used for the assay. Mice were anesthetized with 2% isoflurane, and fur was removed from the back skin in an area of approximately 3 cm in diameter using an electric shaver. Then, 5 μl of a freshly prepared solution containing ICG (0.0075 mg/ml) in Kolliphor HS15 solution (10 mg/ml) was injected intradermally using a 29-gauge insulin syringe. One group of mice was kept anesthetized throughout the experiment, whereas the other group was anesthetized only for the measurement and was allowed to move without any restriction between the measurements.

The fluorescence signal in the back skin was monitored at predetermined time points (0, 1, 2, 3, 4, and 6 hours) with the IVIS system using the following settings: $_{ex}/\lambda_{em}$ = 745/800 nm, exposure time: 1.5 seconds, small binning, field of view: 6.6 cm × 6.6 cm. The average fluorescence intensity in a circular ROI (3 cm in diameter) was analyzed using Living Image Software. Simultaneously, measurements were performed with the custom portable device. After tracer injection, the circular area (3 cm in diameter) around the injection site was marked. The device was moved slightly around the marked injection area until the region of highest intensity was detected. Six measurements were then recorded, and the average of the 3 highest values were used for the data analysis. After subtracting the background readout, the values obtained by each instrument were normalized to the time 0 measurement and plotted against time. The AUC (from 0–4 hours) was calculated for each mouse using a trapezoidal method.

Imaging of tracer uptake into lymphatic and blood vessels. For intravital imaging of lymphatic vessels, a Zeiss StereoLumar.V12 stereomicroscope together with AxioVision software was used. The microscope was equipped with a cooled EMCCD camera (Evolve eXcelon, Photometrics) that has high sensitivity to NIR wavelengths. A high-powered diode system (CoolLED) with illumination at 470–770 nm served as light source. Seven 12- to 19-week-old male FVB mice were used for the imaging. Mice were anesthetized by i.p. injection of 80 mg/kg ketamine and 0.2 mg/kg medetomidine. Fur was removed from the leg with an electric shaver and topical depilation cream. Five μl ICG (0.0075 mg/ml) in Ultrapure water and 10 mg/ml Kolliphor HS15 were injected in the dorsal aspect of the foot using 29-gauge insulin syringes. The collecting lymphatic vessels were observed using a fluorescence stereomicroscope ($\lambda_{ex/em}$ = 770/832 nm, exposure 300 milliseconds, ×40 magnification).

Beginning at 5 minutes after injection, a sequence of 300 images was taken over 2 minutes. Manual compression with a cotton swab was applied onto the injection site for 30 seconds to stimulate uptake of the tracer into blood or lymphatic vessels.

Lymphatic clearance assays in pigs. One domestic pig (number 1, female, 14 kg) was anesthetized with 2% isoflurane throughout the whole experiment. Eight injections of 50 μl freshly prepared ICG (0.0075 mg/ml) in Kolliphor HS15 (10 mg/ml) were performed in the ventral part of the torso using MicronJet600 (NanoPass Technologies Ltd.) microneedles attached to 1 ml BD Luer-Lok syringes. MicronJet600 microneedle-based injection devices, consisting of three 600-μm-long silicon crystal microneedles, have been FDA cleared and CE marked and were tested in many clinical studies of intradermal delivery with various vaccines and compounds (57). Four injections each were placed symmetrically on the left and right

side of the medial line, starting from the pectoral region toward the pelvic part of the ventral torso. The injection sites on the right side were continuously massaged in a circular motion using fingers, starting from 30 minutes after the injection. The signal was measured immediately after each injection and then at 30-minute intervals throughout 4 hours. After the injection, the circular area (3 cm in diameter) around the injection site was marked. For each measurement, the device was moved slightly around the marked injection area in order to localize the region with the highest signal intensity. At every time point, 8–11 measurements at the same injection site were recorded by lifting the device between each measurement. From those data, the 3 highest values were selected for data analysis. Lymphatic clearance was also studied in 2 awake domestic pigs (number 2 and 3, female, 14 and 10 kg, respectively). Each animal was anesthetized with 2% isoflurane, and eight intradermal injections were performed as described above. After the first fluorescence measurement, the anesthesia was removed and each animal was allowed to move without any restrictions. Signal measurements were performed every hour for a total of 4 hours while the animal was manually restrained. Eight to eleven measurements were recorded, and the three highest values were used for the following data analysis.

Statistics. Data are shown as mean ± SD. Means of 2 groups were compared using the 2-tailed Student's *t* test or 2-tailed paired Student's *t* test. Comparisons of 3 groups were performed using 1-way ANOVA with Tukey's multiple comparison post hoc analysis. $P < 0.01$ was considered as significant. GraphPad Prism V7.0 (GraphPad Software) was used for performing the analyses.

Study approval. All mouse experiments were performed in accordance with an animal protocol (ZH212/16) approved by the Cantonal Veterinary Office Zurich, Switzerland. Pig experiments were performed in the Centre National de Biologie Expérimentale, Institute National de la Recherche Scientifique (INRS), Laval, Canada. Procedures involving the care and the use of pigs in this study were reviewed and approved by the INRS Institutional Animal Care and Use Committee (protocol 1711-01) and performed according to the Canadian Council on Animal Care guidelines and policies. Throughout the experiment, the health and well-being of the pigs were closely monitored by a veterinarian.

Author contributions

AKP, MD, JCL, STP, and DB conceived and designed the study. AKP, STP, MD, and JCL wrote the manuscript. AKP and STP performed most experiments and data analyses. MM and SB designed the first prototype of the portable device, and SB built it. DF, MB, and NR designed the final version of the portable device, and DF built it. AKP, TV, and CS performed LC-MS experiments.

Acknowledgments

This work was supported by a Swiss National Science Foundation grant (310030_166490), by funding from the SKINTEGRITY flagship project of the University Medicine Zurich initiative (http://www.hochschulmedizin.uzh.ch/en/projekte/skintegrity.html, funding 2/71018/16), and by Innosuisse – Swiss Innovation Agency (29462.1 IP-LS). NanoPass Technologies Ltd. is acknowledged for providing MicronJet600 microneedles. Mario Filion and the animal caretakers from the Centre National de Biologie Expérimentale, INRS, are acknowledged for support in design and execution of the pig experiments.

Address correspondence to: Michael Detmar, Institute of Pharmaceutical Sciences, ETH Zurich, Vladimir-Prelog-Weg 3, HCI H303, CH-8093 Zurich, Switzerland. Phone: 4144.633.7361; Email: michael.detmar@pharma.ethz.ch.

1. Cueni LN, Detmar M. The lymphatic system in health and disease. *Lymphat Res Biol*. 2008;6(3-4):109–122.
2. Alitalo K. The lymphatic vasculature in disease. *Nat Med*. 2011;17(11):1371–1380.
3. Sayegh HE, et al. Diagnostic methods, risk factors, prevention, and management of breast cancer-related lymphedema: past, present, and future directions. *Curr Breast Cancer Rep*. 2017;9(2):111–121.
4. Bilancini S, Lucchi M, Tucci S, Eleuteri P. Functional lymphatic alterations in patients suffering from lipedema. *Angiology*. 1995;46(4):333–339.
5. Mortimer PS. Evaluation of lymphatic function: abnormal lymph drainage in venous disease. *Int Angiol*. 1995;14(3 Suppl 1):32–35.
6. Saaristo A, et al. Vascular endothelial growth factor-C accelerates diabetic wound healing. *Am J Pathol*. 2006;169(3):1080–1087.
7. Jurisic G, Sundberg JP, Detmar M. Blockade of VEGF receptor-3 aggravates inflammatory bowel disease and lymphatic vessel enlargement. *Inflamm Bowel Dis*. 2013;19(9):1983–1989.
8. Guo R, et al. Inhibition of lymphangiogenesis and lymphatic drainage via vascular endothelial growth factor receptor

3 blockade increases the severity of inflammation in a mouse model of chronic inflammatory arthritis. *Arthritis Rheum*. 2009;60(9):2666–2676.
9. Huggenberger R, Ullmann S, Proulx ST, Pytowski B, Alitalo K, Detmar M. Stimulation of lymphangiogenesis via VEGFR-3 inhibits chronic skin inflammation. *J Exp Med*. 2010;207(10):2255–2269.
10. Tassenoy A, De Strijcker D, Adriaenssens N, Lievens P. The use of noninvasive imaging techniques in the assessment of secondary lymphedema tissue changes as part of staging lymphedema. *Lymphat Res Biol*. 2016;14(3):127–133.
11. Modi S, Stanton AW, Mortimer PS, Levick JR. Clinical assessment of human lymph flow using removal rate constants of interstitial macromolecules: a critical review of lymphoscintigraphy. *Lymphat Res Biol*. 2007;5(3):183–202.
12. Mortimer PS, Simmonds R, Rezvani M, Robbins M, Hopewell JW, Ryan TJ. The measurement of skin lymph flow by isotope clearance--reliability, reproducibility, injection dynamics, and the effect of massage. *J Invest Dermatol*. 1990;95(6):677–682.
13. Modi S, Stanton AW, Svensson WE, Peters AM, Mortimer PS, Levick JR. Human lymphatic pumping measured in healthy and lymphoedematous arms by lymphatic congestion lymphoscintigraphy. *J Physiol (Lond)*. 2007;583(Pt 1):271–285.
14. Fowler JC, et al. Measurement of lymph node function from the extraction of immunoglobulin in lymph. *Scand J Clin Lab Invest*. 2010;70(2):112–115.
15. Frangioni JV. In vivo near-infrared fluorescence imaging. *Curr Opin Chem Biol*. 2003;7(5):626–634.
16. Karlsen TV, McCormack E, Mujic M, Tenstad O, Wiig H. Minimally invasive quantification of lymph flow in mice and rats by imaging depot clearance of near-infrared albumin. *Am J Physiol Heart Circ Physiol*. 2012;302(2):H391–H401.
17. Karaman S, Buschle D, Luciani P, Leroux JC, Detmar M, Proulx ST. Decline of lymphatic vessel density and function in murine skin during aging. *Angiogenesis*. 2015;18(4):489–498.
18. Bunschoten A, et al. Targeted non-covalent self-assembled nanoparticles based on human serum albumin. *Biomaterials*. 2012;33(3):867–875.
19. Li X, Fu Y, Ma L, Wang Z, Zhang H. Spectrometric study on the interaction of indocyanine green with human serum albumin. *Chem Res Chin Univ*. 2016;32(3):343–347.
20. Brambilla D, Proulx ST, Marschalkova P, Detmar M, Leroux JC. Microneedles for the noninvasive structural and functional assessment of dermal lymphatic vessels. *Small*. 2016;12(8):1053–1061.
21. Gashev AA, Nagai T, Bridenbaugh EA. Indocyanine green and lymphatic imaging: current problems. *Lymphat Res Biol*. 2010;8(2):127–130.
22. Proulx ST, et al. Quantitative imaging of lymphatic function with liposomal indocyanine green. *Cancer Res*. 2010;70(18):7053–7062.
23. Weiler M, Kassis T, Dixon JB. Sensitivity analysis of near-infrared functional lymphatic imaging. *J Biomed Opt*. 2012;17(6):066019.
24. Unno N, et al. Quantitative lymph imaging for assessment of lymph function using indocyanine green fluorescence lymphography. *Eur J Vasc Endovasc Surg*. 2008;36(2):230–236.
25. Tagaya N, et al. Intraoperative identification of sentinel lymph nodes by near-infrared fluorescence imaging in patients with breast cancer. *Am J Surg*. 2008;195(6):850–853.
26. Reekers M, et al. Cardiovascular monitoring by pulse dye densitometry or arterial indocyanine green dilution. *Anesth Analg*. 2009;109(2):441–446.
27. Levesque E, et al. Plasma disappearance rate of indocyanine green: a tool to evaluate early graft outcome after liver transplantation. *Liver Transpl*. 2009;15(10):1358–1364.
28. Werner SG, et al. Inflammation assessment in patients with arthritis using a novel in vivo fluorescence optical imaging technology. *Ann Rheum Dis*. 2012;71(4):504–510.
29. Göröcs Z, et al. Quantitative fluorescence sensing through highly autofluorescent, scattering, and absorbing media using mobile microscopy. *ACS Nano*. 2016;10(9):8989–8999.
30. Young CM, Hopewell JW. The evaluation of an isotope clearance technique in the dermis of pig skin: a correlation of functional and morphological parameters. *Microvasc Res*. 1980;20(2):182–194.
31. Norman JJ, et al. Reliability and accuracy of intradermal injection by Mantoux technique, hypodermic needle adapter, and hollow microneedle in pigs. *Drug Deliv Transl Res*. 2014;4(2):126–130.
32. Kim YC, Park JH, Prausnitz MR. Microneedles for drug and vaccine delivery. *Adv Drug Deliv Rev*. 2012;64(14):1547–1568.
33. Babity S, Roohnikan M, Brambilla D. Advances in the design of transdermal microneedles for diagnostic and monitoring applications. *Small*. 2018;14(49):e1803186.
34. Bégu S, Devoisselle JM, Mordon S. Noninvasive fluorescent study in situ and in real time of glucose effects on the pharmacokinetic of calcein. *J Biomed Opt*. 2002;7(4):609–612.
35. Mordon S, Devoisselle JM, Soulie-Begu S, Desmettre T. Indocyanine green: physicochemical factors affecting its fluorescence in vivo. *Microvasc Res*. 1998;55(2):146–152.
36. Kraft JC, Ho RJ. Interactions of indocyanine green and lipid in enhancing near-infrared fluorescence properties: the basis for near-infrared imaging in vivo. *Biochemistry*. 2014;53(8):1275–1283.
37. Kirchherr AK, Briel A, Mäder K. Stabilization of indocyanine green by encapsulation within micellar systems. *Mol Pharm*. 2009;6(2):480–491.
38. Meyer J, et al. In vivo imaging of a new indocyanine green micelle formulation in an animal model of laser-induced choroidal neovascularization. *Invest Ophthalmol Vis Sci*. 2014;55(10):6204–6212.
39. Zhang H, Wang Z, Liu O. Simultaneous determination of Kolliphor HS15 and miglyol 812 in microemulsion formulation by ultra-high performance liquid chromatography coupled with nano quantity analyte detector. *J Pharm Anal*. 2016;6(1):11–17.
40. Lu H, Li J, Li M, Gong T, Zhang Z. Systemic delivery of alpha-asarone with Kolliphor HS 15 improves its safety and therapeutic effect on asthma. *Drug Deliv*. 2015;22(3):266–275.
41. Saxena V, Sadoqi M, Shao J. Degradation kinetics of indocyanine green in aqueous solution. *J Pharm Sci*. 2003;92(10):2090–2097.
42. Mindt S, Karampinis I, John M, Neumaier M, Nowak K. Stability and degradation of indocyanine green in plasma, aqueous solution and whole blood. *Photochem Photobiol Sci*. 2018;17(9):1189–1196.
43. Barbier F, DeWeerdt GA. Chromatography and I.R. spectrography of indocyanine green. *Clin Chim Acta*. 1964;10:549–554.

44. Ott P. Hepatic elimination of indocyanine green with special reference to distribution kinetics and the influence of plasma protein binding. *Pharmacol Toxicol*. 1998;83 Suppl 2:1–48.
45. Yan L, Qiu L. Indocyanine green targeted micelles with improved stability for near-infrared image-guided photothermal tumor therapy. *Nanomedicine (Lond)*. 2015;10(3):361–373.
46. Rodriguez VB, Henry SM, Hoffman AS, Stayton PS, Li X, Pun SH. Encapsulation and stabilization of indocyanine green within poly(styrene-alt-maleic anhydride) block-poly(styrene) micelles for near-infrared imaging. *J Biomed Opt*. 2008;13(1):014025.
47. Narang AS, Rao VM, Desai DS. Effect of antioxidants and silicates on peroxides in povidone. *J Pharm Sci*. 2012;101(1):127–139.
48. Wu Y, Levons J, Narang AS, Raghavan K, Rao VM. Reactive impurities in excipients: profiling, identification and mitigation of drug-excipient incompatibility. *AAPS PharmSciTech*. 2011;12(4):1248–1263.
49. Mäkinen T, et al. Inhibition of lymphangiogenesis with resulting lymphedema in transgenic mice expressing soluble VEGF receptor-3. *Nat Med*. 2001;7(2):199–205.
50. Tagaya N, et al. Intraoperative identification of sentinel lymph nodes by near-infrared fluorescence imaging in patients with breast cancer. *Am J Surg*. 2008;195(6):850–853.
51. Proulx ST, Ma Q, Andina D, Leroux JC, Detmar M. Quantitative measurement of lymphatic function in mice by noninvasive near-infrared imaging of a peripheral vein. *JCI Insight*. 2017;2(1):e90861.
52. Stanton AW, et al. Impairment of lymph drainage in subfascial compartment of forearm in breast cancer-related lymphedema. *Lymphat Res Biol*. 2003;1(2):121–132.
53. Swindle MM, Makin A, Herron AJ, Clubb FJ, Frazier KS. Swine as models in biomedical research and toxicology testing. *Vet Pathol*. 2012;49(2):344–356.
54. Meyer W, Schwarz R, Neurand K. The skin of domestic mammals as a model for the human skin, with special reference to the domestic pig. *Curr Probl Dermatol*. 1978;7:39–52.
55. Ito R, Suami H. Lymphatic territories (lymphosomes) in swine: an animal model for future lymphatic research. *Plast Reconstr Surg*. 2015;136(2):297–304.
56. Sumena KB, Lucy KM, Chungath JJ, Ashok N, Harshan KR. Morphology of the skin in large white Yorkshire pigs. *Indian J Anim Res*. 2010;44(1):55–57.
57. Levin Y, Kochba E, Hung I, Kenney R. Intradermal vaccination using the novel microneedle device MicronJet600: Past, present, and future. *Hum Vaccin Immunother*. 2015;11(4):991–997.
58. Proulx ST, et al. Use of a PEG-conjugated bright near-infrared dye for functional imaging of rerouting of tumor lymphatic drainage after sentinel lymph node metastasis. *Biomaterials*. 2013;34(21):5128–5137.
59. Modi S, Stanton AW, Mellor RH, Peters AM, Levick JR, Mortimer PS. Regional distribution of epifascial swelling and epifascial lymph drainage rate constants in breast cancer-related lymphedema. *Lymphat Res Biol*. 2005;3(1):3–15.
60. Negrini D, Moriondo A. Lymphatic anatomy and biomechanics. *J Physiol (Lond)*. 2011;589(Pt 12):2927–2934.
61. Swartz MA, et al. Mechanics of interstitial-lymphatic fluid transport: theoretical foundation and experimental validation. *J Biomech*. 1999;32(12):1297–1307.
62. Ellis JP, Marks R, Perry BJ. Lymphatic function: the disappearance rate of 131-I albumin from the dermis. *Br J Dermatol*. 1970;82(6):593–599.
63. Wissenbach DK, Meyer MR, Remane D, Philipp AA, Weber AA, Maurer HH. Drugs of abuse screening in urine as part of a metabolite-based LC-MSn screening concept. *Anal Bioanal Chem*. 2011;400(10):3481–3489.
64. Bachmann SB, Detmar M, Proulx ST. Visualization and measurement of lymphatic function in vivo. *Methods Mol Biol*. 2018;1846:197–211.